Chapter 5

The combinatorial background

One of the most important contributions to the intermediate mass region (IMR) opposite-sign dimuon spectra is the background from pion and kaon decays. Its contribution to the IMR mass spectrum amounts up to 85% in p-A collisions at 450 GeV/c and S-U collisions at 200 A GeV/c and to 95% in the most central Pb-Pb collisions at 158 A GeV/c. To study the IMR dimuon sources and their behaviour with changing energy and centrality of the collision, the combinatorial background has to be subtracted in such a way that no doubts remain about the nature of the measured signal. There exist widely used methods to evaluate the combinatorial background shape basically starting from the experimental like-sign background distributions. The normalisation of the background contribution to the opposite-sign dimuon spectrum can also be extracted using the same methods, if we are dealing with interactions where the produced high particle multiplicities simulate the absence of charge correlation effects. When charge correlation effects can not be neglected, they have to be carefully estimated to eventually correct the background normalisation factor.

The first part of this chapter describes the commonly used methods for the determination of the opposite-sign combinatorial background mass differential distribution and normalisation, when charge correlation effects can be neglected. The second part presents the detailed description of the Monte-Carlo simulation used in this work to estimate the charge correlation effects on the background normalisation factor.

5.1 The background shape and normalisation

The background contribution to the opposite-sign dimuon mass spectrum is usually evaluated using the like-sign dimuon mass distributions. This is due to the fact that the π and K meson decays,

$$\pi^{+}(or K^{+}) \longrightarrow \mu^{+}\nu \tag{5.1}$$

and

$$\pi^{-}(or K^{-}) \longrightarrow \mu^{-}\overline{\nu} \tag{5.2}$$

contribute both to the opposite and to the like-sign spectra. While the opposite-sign distribution is the superposition of many different sources, the like-sign distributions are purely due to combinatorial background.
The background computation is based on the following reasoning[1] : consider a set of N_0 dimuon events. If each primary interaction produces N^+ positive mesons and N^- negative ones, with the associated $P(N^+)$ and $P(N^-)$ muon decay probabilities, the number of produced like-sign dimuons is

$$N^{++} = N_0 \int A^{++} \frac{dP(N^+)}{dN^+} \frac{N^+(N^+-1)}{2} dN^+ = \frac{N_0}{2}(< N^{+^2} > - < N^+ >)A^{++} \tag{5.3}$$

where A^{++} is the acceptance for positive like-sign dimuons. The same holds for negative like-sign dimuons. If the numbers N^+ and N^- of produced positive and negative mesons are uncorrelated, the number of opposite-sign dimuons resulting from the combination of their decay products can be written as

$$N^{+-} = N_0 \int A^{+-} \frac{dP(N^+)}{dN^+} \frac{dP(N^-)}{dN^-} N^+ N^- dN^+ dN^- = N^0 < N^+ >< N^- > A^{+-} \tag{5.4}$$

where A^{+-} is the acceptance for opposite-sign dimuons.
Since the meson multiplicity follows the Poisson law, which implies

$$< N >=< N^2 > - < N >^2 \tag{5.5}$$

we can easily obtain

$$N^{+-} = 2\sqrt{N^{++}N^{--}} \cdot \frac{A^{+-}}{\sqrt{A^{++}A^{--}}} \tag{5.6}$$

If the acceptance is the same for positive and negative muons, condition which is fulfilled in NA38/NA50 because of the image cut imposed on the data at processing time (see chapter 3), we can write

$$N^{+-} = 2\sqrt{N^{++}N^{--}} \tag{5.7}$$

In NA50, to correct for a possible image cut inefficiency, the sign of the magnetic field is regularly changed in order to have a set of data of equal statistics for both magnetic field sign. This means that eq.5.7 has to be modified in

$$N^{+-} = 2\left\{\sqrt{(N^{++}N^{--})_{(+)}} + \sqrt{(N^{++}N^{--})_{(-)}}\right\} \tag{5.8}$$

Eq.5.8 is strictly valid only for events where the meson production is completely charge uncorrelated. This is of course not the case in the real physical situation, where positively and negatively charged mesons are linked by the total charge conservation law. On the other hand, when the multiplicity of charged particles generated in the interaction is so large that the existing physical charge correlation is smeared out, eq.5.8 is still valid. This is the case for very central Pb-Pb collisions, whilst charge correlation effects are still expected in the peripheral ones. When it perfectly holds, eq.5.8 defines the shape and normalisation of the background contribution. Otherwise, if it is necessary to correct for charge correlation effects, eq.5.8 has to be multiplied by an R factor which is expected to be equal to 1 in very central A-B collisions and larger than 1 in p-A or peripheral A-B collisions,

$$N^{+-} = 2R_{bck}\left\{\sqrt{(N^{++}N^{--})_{(+)}} + \sqrt{(N^{++}N^{--})_{(-)}}\right\} \tag{5.9}$$

In fig.5.1 the like-sign dimuon distributions and in fig.5.2 the resulting opposite-sign distribution are shown for the pAl set of data for R_{BCK}=1.
The above described technique for the determination of the combinatorial background differential distribution and normalisation, is from now on referred to as the 2sqrt method.

5.1.1 The FOS method

The FOS (Fake Opposite Sign)[2] method is used to compute the shape of the combinatorial background contribution when a better degree of accuracy is needed. Therefore, it has been used in the analysis of the PbPb set of data which is characterized by a very large background contribution to the IMR.
The PbPb set of data has been subdivided in subsamples corresponding to the 9 E_T bins used in the analysis (see chapter 3). Within each of this subsamples, or class of events, the positive and negative single muon distributions are extracted from the

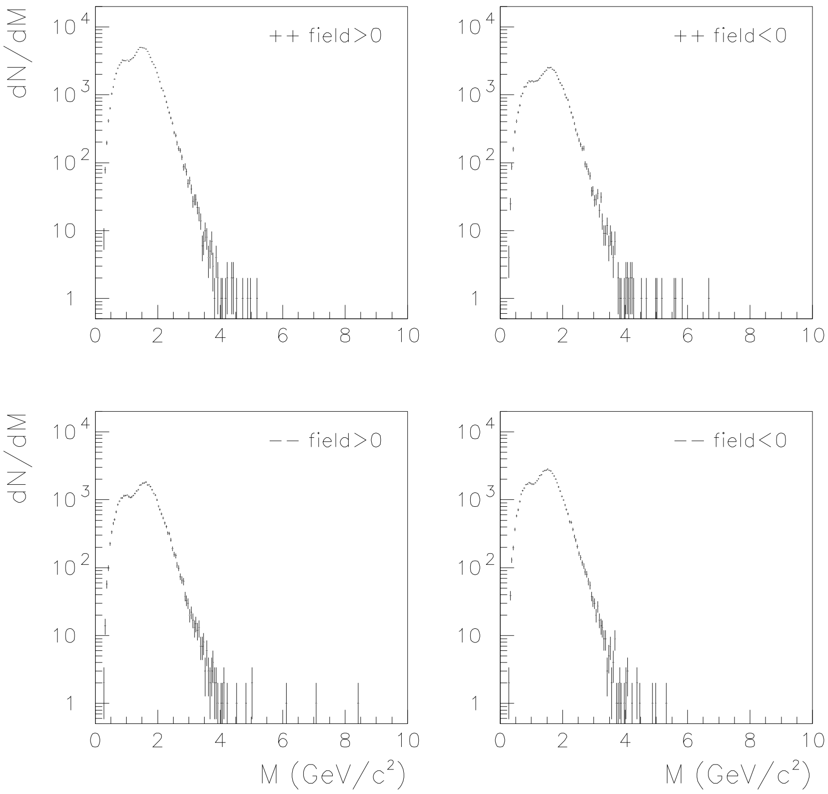

Figure 5.1: *Like sign dimuon distributions for the pAl set of data.*

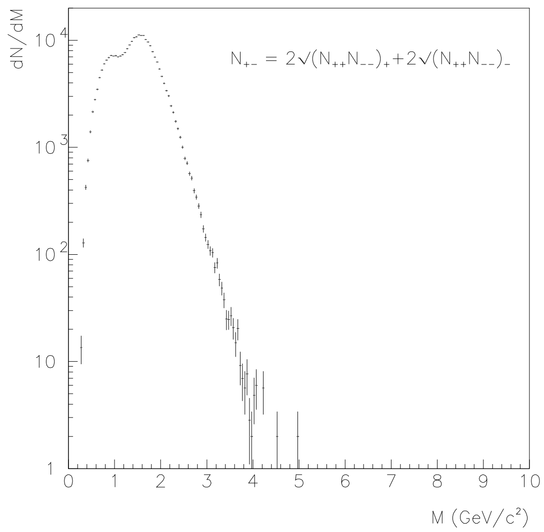

Figure 5.2: *OS Background calculated with the 2sqrt method (R_{bck}=1) for the pAl set of data.*

like-sign ones. The single muon momenta are stored for each class of events. Within each class of events, all the single muon combinations allowed by the trigger are made. The resulting spectra can then be normalised using eq.5.9, where the total quantities N^{++} and N^{--} are known.
The validity of this method has been checked by the authors. In ref.[2], where a detailed description of the method can be found, the like-sign dimuon distributions have been reconstructed from the single muon ones; they have then been compared with the experimental like-sign mass distributions and a satisfactory agreement has been found.
In fig.5.3 the difference in the background shape determination as obtained with the FOS and 2sqrt methods is shown for the second, very peripheral, PbPb E_T bin. Eq.5.9, with R_{BCK}=1, has been used to normalise. The difference is well evident when subtracting the background contribution from the total opposite-sign mass spectrum, obtaining the so called signal mass distribution. In fig.5.4 the same is shown for the PbPb most central E_T bin. When the FOS method is used, the signal distribution is smoother than when using the usual 2sqrt method; this is the reason why the former has been adopted for the PbPb system.

5.2 The R_{BCK} factor

Up to now, within the NA38/NA50 Collaboration, the R_{BCK} factor was either obtained from the fit of the mass spectrum, where it was left as a free parameter, or it was imposed equal to 1 in all the nucleus-nucleus interactions. This last approximation turns out to be applicable if the region of mass $M > 2.8\ GeV/c^2$ is under study, since the background contribution in the high mass region is very small.
On the other hand, in the IMR the combinatorial background appears to be the most important contribution as shown in fig.5.5 for the PbPb, SU and pW systems. A precise calculation of the R_{BCK} factor is therefore needed.
In the following I give a detailed description of the Monte-Carlo simulation used to compute the R_{BCK} factors for all the analysed systems.

5.2.1 Pion and kaon distributions from VENUS

Using the VENUS 4.02[4] event generator, a large number ($\simeq 4 \cdot 10^5$)of p-A, S-U and Pb-Pb events, at the relevant energies, have been generated. For each system, the produced pions and kaons, and the related kinematic variable values, have been stored. As an example, fig.5.6 shows the π and K energy distributions versus the pseudo-rapidity η as obtained from VENUS in p-W events at 450 GeV/c. The shaded areas correspond to the region outside the apparatus angular acceptance.
Once the pions and kaons produced by VENUS have been stored, they are tracked through the NA50 hadron absorber and there forced to decay. A decay probability is associated to each of them with the following reasoning :

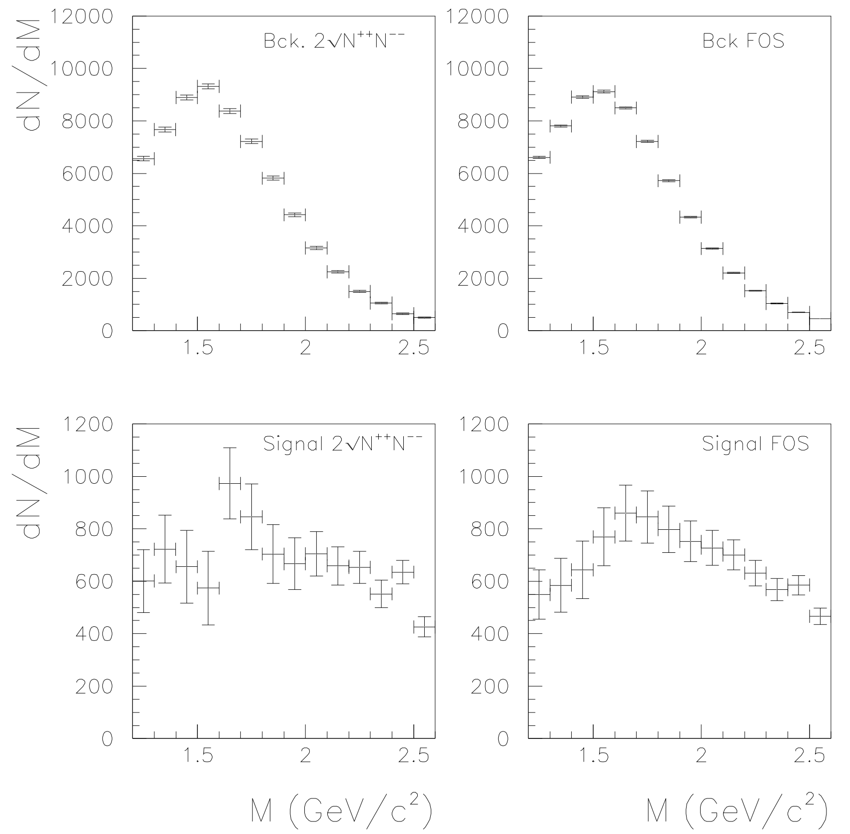

Figure 5.3: *Comparison between the 2sqrt (R_{bck}=1) and FOS background computation on the 2^{nd} PbPb E_T bin and the resulting signals, defined as the total opposite-sign dimuon mass distribution subtracted for the combinatorial background.*

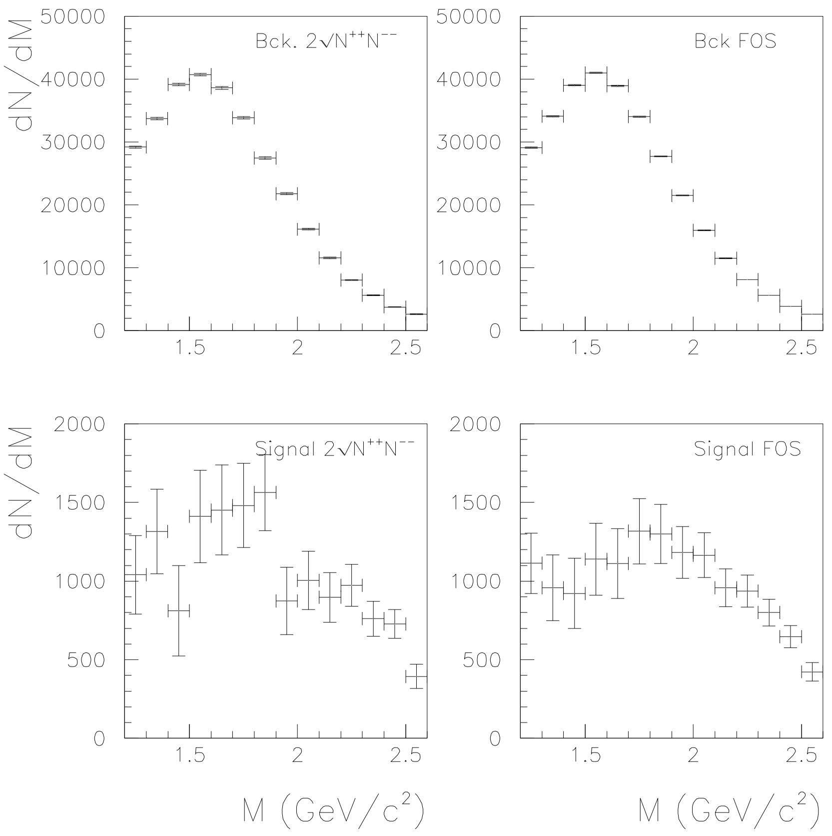

Figure 5.4: *Same as fig.5.3 but for the most central PbPb E_T bin (R_{bck}=1).*

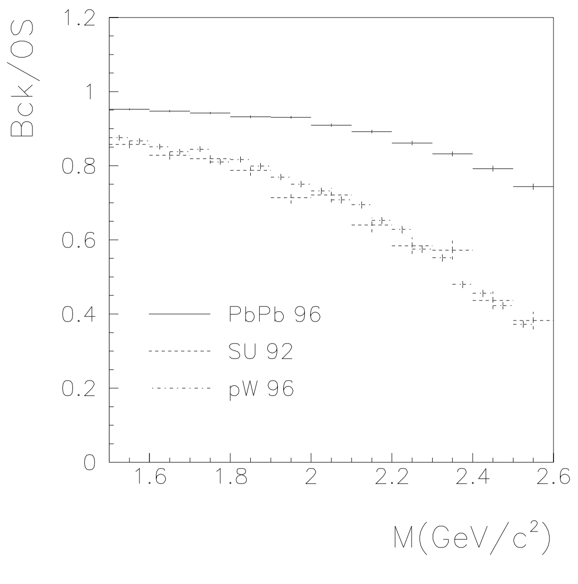

Figure 5.5: *Ratio of combinatorial background and total opposite-sign dimuon mass distribution in the IMR and for the three shown systems, when R_{bck}=1.*

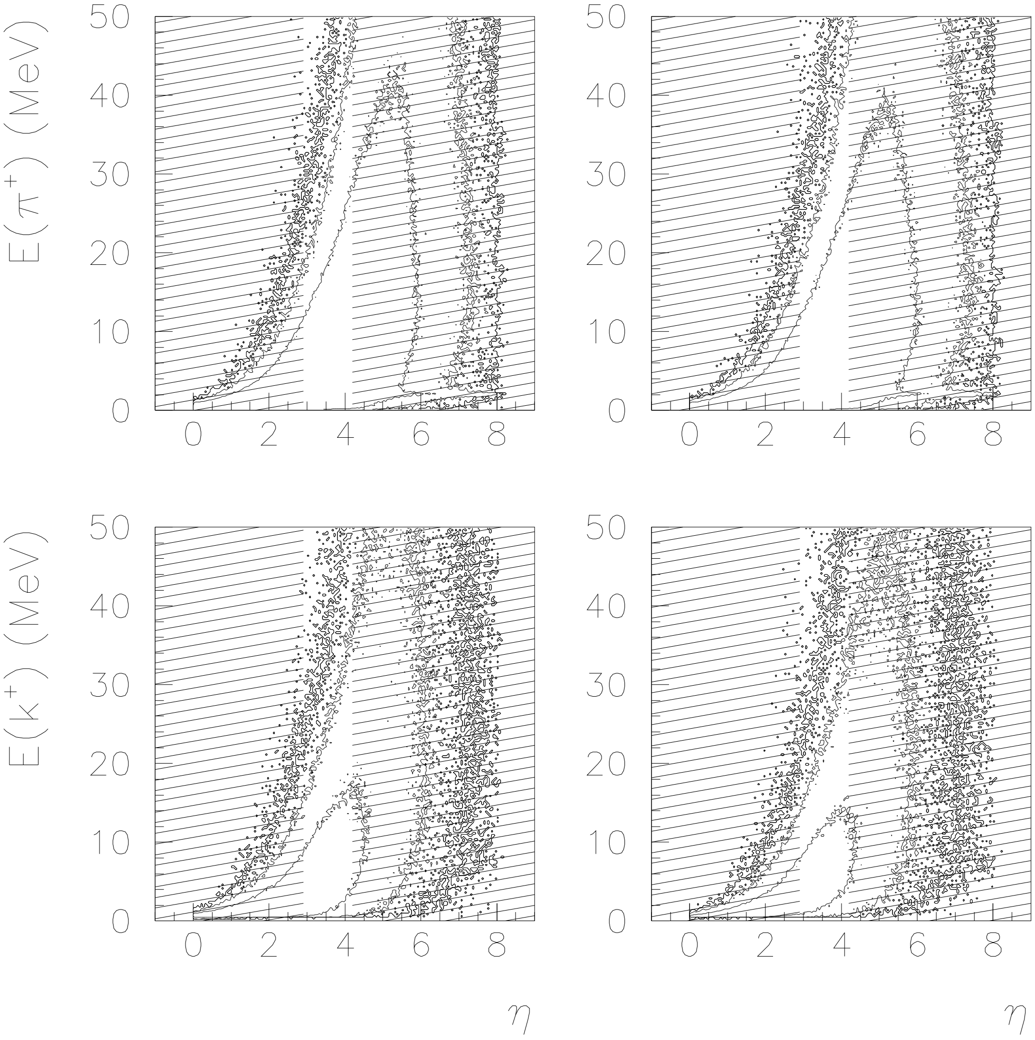

Figure 5.6: *Pion and kaon energy distribution vs. η as produced by VENUS in p-W events at 450 GeV/c. The shaded areas correspond to the region outside the apparatus angular acceptance.*

- Suppose a meson has been generated at $x = 0$; its probability of having survived up until the point x_0 without undergoing an hadronic interaction is

$$P^h(x_0) = e^{(-x_0/\lambda_i)} \tag{5.10}$$

where λ_i is the hadronic interaction length in cm if x is measured in cm.

- If the meson has survived up until the point x_0, the differential probability that it decays between x_0 and $x_0 + dx$ is

$$\frac{dP^d(x)}{dx}\mid_{x_0} = \frac{Mc}{p(x_0) \cdot X_L} \cdot e^{\frac{(-Mcx_0)}{(p(x_0)X_L)}} \ (cm^{-1}) \tag{5.11}$$

where M (GeV/c^2) is the meson mass, c is the velocity of light, X_L=τc (cm) where τ (s) is the meson mean life time and $p(x_0)$ (GeV/c) is the meson momentum at the point x_0,

$$p(x_0) = \sqrt{E^2(x_0) - M^2} \ (GeV/c) \tag{5.12}$$

with

$$E(x_0) = E(0) - \Delta E \ (GeV) \tag{5.13}$$

where $E(0)$ is the energy the meson had at production and $\Delta E(x)$ is the energy lost by the meson between x=0 and x_0,

$$\Delta E = \int_0^{x_0} \frac{dE}{dx} dx \ (GeV) \tag{5.14}$$

where dE/dx is the energy loss in GeV/cm.

- The differential probability for a meson produced at $x = 0$ to decay at x_0 is given by the combined probability

$$\frac{dP^{hd}(x)}{dx}\mid_{x_0} = P^h(x_0) \cdot \frac{dP^d(x)}{dx}\mid_{x_0} \ (cm^{-1}) \tag{5.15}$$

Material	Length (cm)	λ_i (g/cm^2)	ρ (g/cm^3)
Air	25.4	84.40	1.2
Al_2O_3	51.6	98.70	3.82
BeO	59.0	84.90	2.81
C	400.	86.30	1.93

Table 5.1: *Characteristics of the materials crossed by pions and kaons when going through the hadron absorber.*

- The decay probability $P^{hd}(x_i)$ is computed at each discrete point x_i along the meson path. The decay probability at the point x_i is strictly connected with the material where the point x_i is and with the previously crossed materials. Globally, each meson has to cross 25.4 cm of air followed by 51.6 cm of Al_2O_3 (or 59 cm of BeO in PbPb and pW) and then 400 cm of C. The decay probability $P^{hd}(x_i)$ is computed in steps of 1 cm. Table.5.1 lists the length, interaction length and density of the hadron absorber materials. All mesons which did not decay within the above listed materials, are considered to be stopped in the last 80 cm of Fe.

  The total decay probability for a single meson j is then given by

$$P_j^{tot} = \int_0^{L_{abs}} \frac{dP_j^{hd}(x)}{dx} dx \tag{5.16}$$

where L_{abs} is the total absorber plus pre-absorber length.
The calculated decay probabilities are then used as relative weights in the π and K distributions.

5.2.2 Monte-Carlo dimuon distributions

The next step consists in the combination of the generated mesons, which are then forced to decay. Within each VENUS event, every single pion and kaon is combined with all the other produced mesons in the same event. This means that the same meson is used $N_e - 1$ times for combination if N_e is the total number of stored mesons in a single VENUS event. Next, the mesons are forced to decay into a muon; this is accomplished using the two body decay process with isotropic angular distribution in the centre of mass frame[5]. The kinematic variables (rapidity y, polar and azimuthal angle in the Collin-Soper frame, transverse momentum p_T, invariant mass) of the resulting dimuons are then computed. Each dimuon is weighted by the product of the decay probabilities of its two parents,

$$P^{ab}_{jk} = P^a_j P^b_k \tag{5.17}$$

with ab = (−−) or (++) or (+−) and j,k=1....N_e

In fig.5.7 the weight distribution obtained for π's and K's pairs in semi-peripheral (b=10 fm) Pb-Pb interactions at 158 A GeV/c is shown.

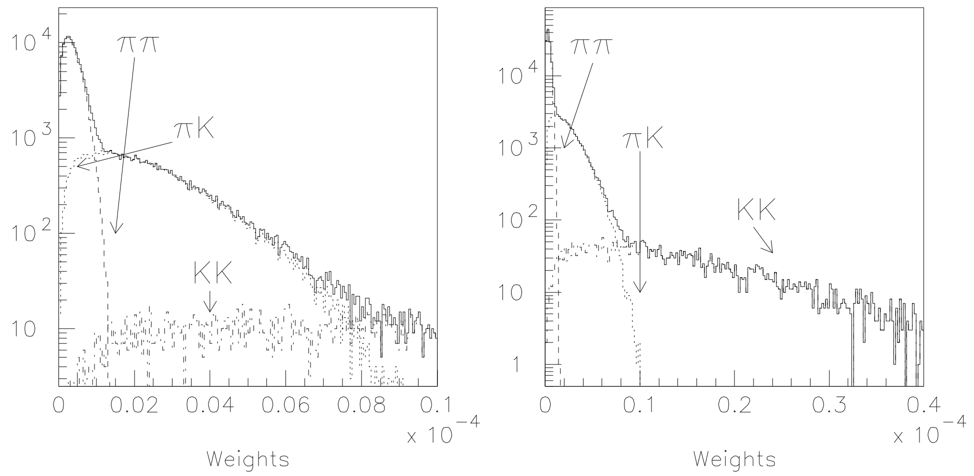

Figure 5.7: *Weights associated to pion and kaon pairs resulting from the combination of π's and K's produced by VENUS in Pb-Pb collisions at 158 GeV/c per nucleon. The small probabilities region is better shown in the left panel.*

Of all the created dimuons, only the ones falling in the apparatus acceptance are kept. We thus apply on the dimuon distributions the following cuts :

1. At the dimuon level

   The usual rapidity and $cos\theta_{CS}$ cuts,

$$3 < y_{lab} < 4 \tag{5.18}$$

$$-0.5 < cos\theta_{CS} < 0.5 \tag{5.19}$$

2. On single muons

   A cut which approximates the single muon angular and energy acceptance of the muon spectrometer can be obtained from experimental data. In fig.5.8 the muon energy versus the muon angle θ_μ is shown as deduced from the NA38 and NA50 experimental data. The muon angle θ_μ is defined as

$$\theta_\mu = tan^{-1}(\frac{p_T}{p_l}) \tag{5.20}$$

where p_T and p_l are the transverse and longitudinal momenta of the muon at the point where its parent decay takes place. In fig.5.8 the region in the E_μ-θ_μ plane corresponding to accepted muons can be individuated; the shown regions can be delimited with the following cuts,

- NA50
  $E_\mu > 8.$ GeV for $0.065 \leq \theta_\mu \leq 0.090$
  $E_\mu > 16000\ (\theta_\mu - 0.065)^2 + 8.$ GeV for $0.037 \leq \theta_\mu < 0.065$
  $E_\mu > 13000\ (\theta_\mu - 0.090)^2 + 8.$ GeV for $0.090 < \theta_\mu \leq 0.108$
- NA38
  $E_\mu > 2.5$ GeV for $0.070 \leq \theta_\mu \leq 0.080$
  $E_\mu > 13000\ (\theta_\mu - 0.070)^2 + 2.5$ GeV for $0.032 \leq \theta_\mu < 0.070$
  $E_\mu > 13000\ (\theta_\mu - 0.080)^2 + 2.5$ GeV for $0.080 < \theta_\mu \leq 0.102$

The defined acceptance cut is then applied on the Monte-Carlo generated muons. This last cut is only imposed to muons belonging to dimuons which survived the y and $cos\theta_{CS}$ cut previously applied.

In fig.5.9 the resulting dimuon mass, rapidity, p_T and $cos\theta_{CS}$ distributions are shown for peripheral (b=10 fm) Pb-Pb events at 158 GeV/c per nucleon, before kinematic cuts. In fig.5.10 the same is shown after kinematic cuts have been applied. The difference in the binning of the two plots is due to the reduced statistics after kinematic cuts.

5.2.3 R_{BCK} factor from dimuon Monte-Carlo distributions

From the histograms for the dimuon mass, p_T, rapidity and $cos\theta_{CS}$ distributions, the R_{BCK} factor can be extracted as a function of the dimuon kinematic variables. For each value x in the distribution of the kinematic variable X (X=p_T, y, M, $cos\theta_{CS}$), we can write

$$R_{Monte-Carlo}(x) = \frac{\sum_{n=1}^{N_V} \sum_{i,j} P^{+-}(x)_{i,j}}{2\sqrt{(\sum_{n=1}^{N_V} \sum_{i,j} P^{++}(x)_{i,j})(\sum_{n=1}^{N_V} \sum_{i,j} P^{--}(x)_{i,j})}} \tag{5.21}$$

where N_V is the total number of produced VENUS events and $i, j = 1....N_e$ if N_e is the number of produced mesons in the VENUS event e.

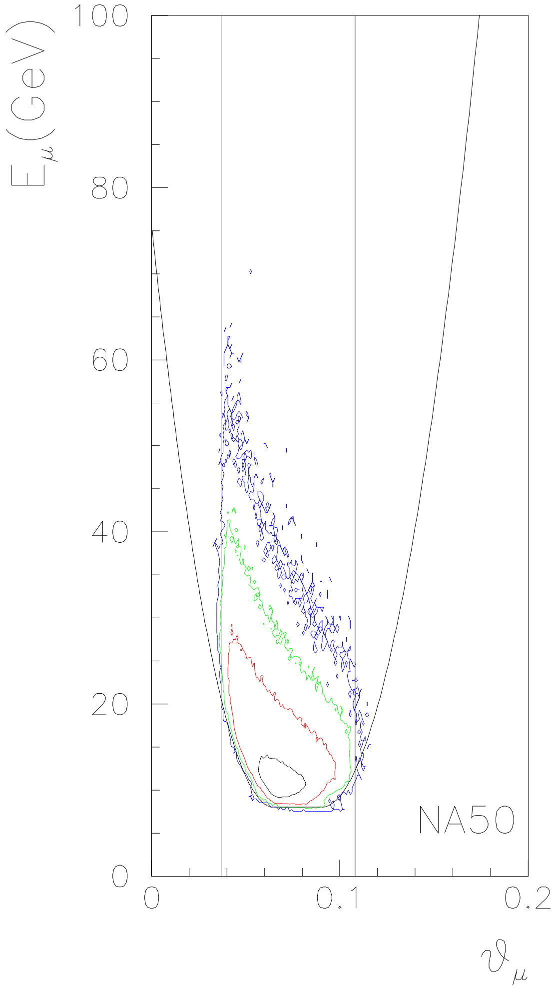

Figure 5.8: *Muon energy vs. muon polar angle as deduced from NA50 and NA38 data. The delimited areas correspond to the acceptance cut imposed to the Monte-Carlo single muon distributions to simulate the tracking of the muons through the whole muon spectrometer.*

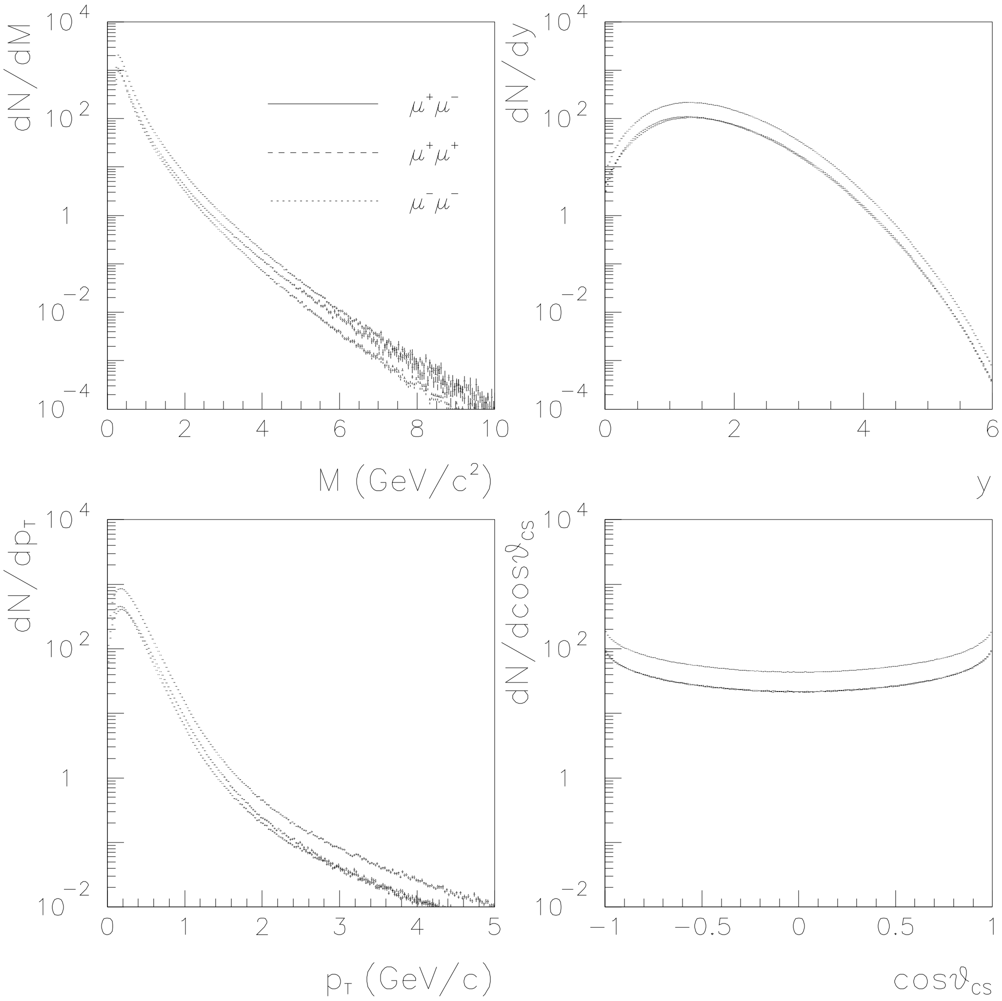

Figure 5.9: *Differential distributions of Monte-Carlo generated dimuon kinematic variables* before *kinematic cuts for peripheral (b=10 fm) Pb-Pb events at 158 A GeV/c.*

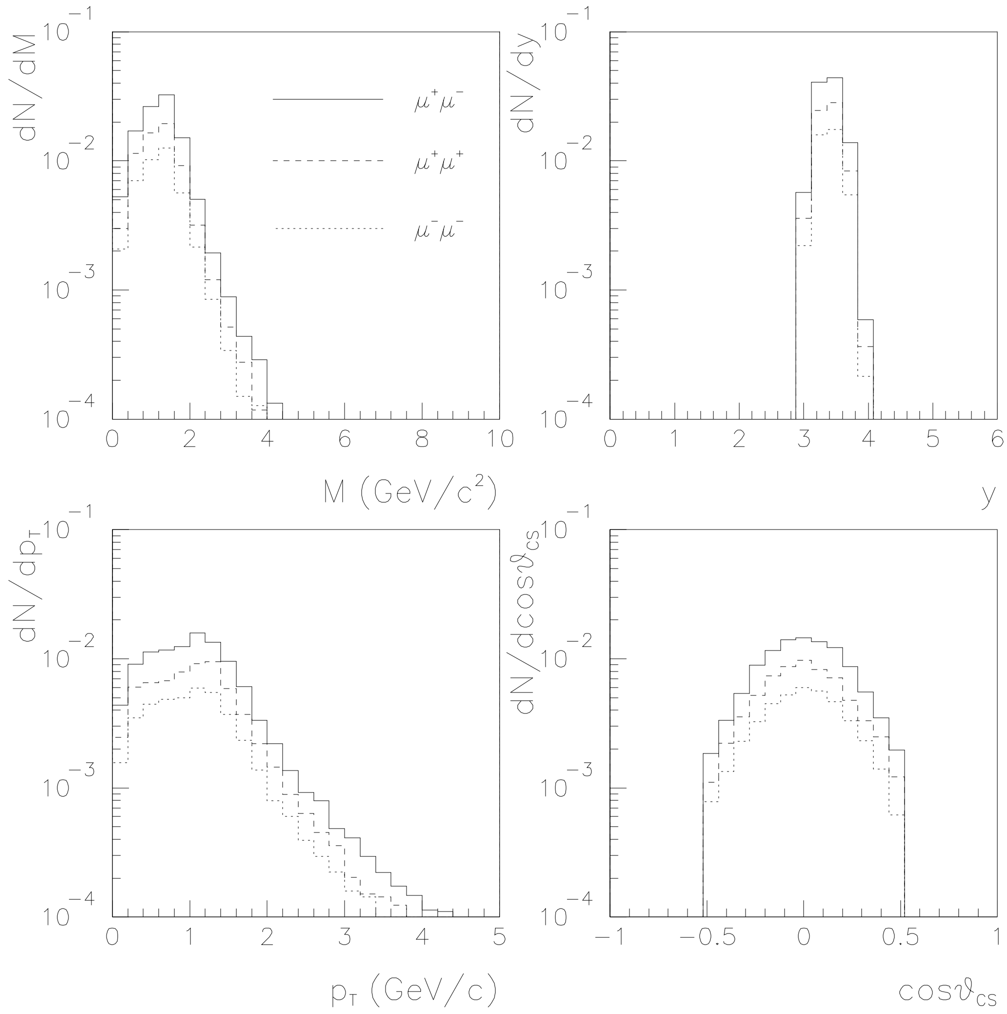

Figure 5.10: *Differential distributions of Monte-Carlo generated dimuon kinematic variables* after *kinematic cuts for peripheral (b=10 fm) Pb-Pb events at 158 A GeV/c.*

In other words, the ratio $N_{+-}^{Monte-Carlo}/2\sqrt{N_{++}^{Monte-Carlo}N_{--}^{Monte-Carlo}}$ is calculated bin per bin for each of the dimuon variables. In fig.5.11 the R_{BCK} factor distribution as a function of the dimuon mass, rapidity, p_T and $cos\theta_{CS}$ is shown for peripheral (b=10 fm) Pb-Pb 158 A GeV/c events. Kinematic cuts have not been applied.
In fig.5.12, where kinematic cuts have been applied, the R_{BCK} factor does not show any strong dependence on the dimuon kinematic variables.

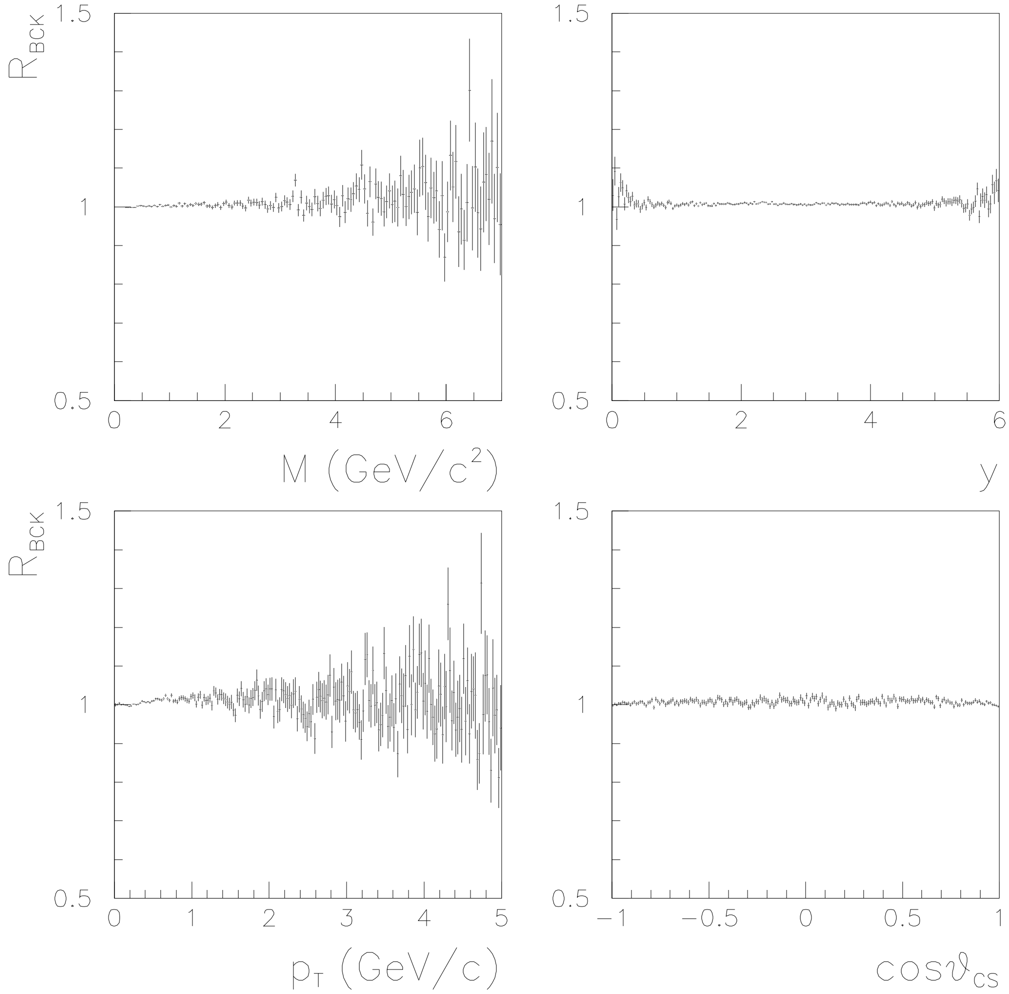

Figure 5.11: *Monte-Carlo R_{BCK} factor vs. dimuon mass, y, p_T and $cos\theta_{CS}$* before *kinematic cuts for peripheral (b=10 fm) Pb-Pb 158 A GeV/c events.*

To compute the average R_{BCK} value we then integrate over the dimuon kinematic variable distributions

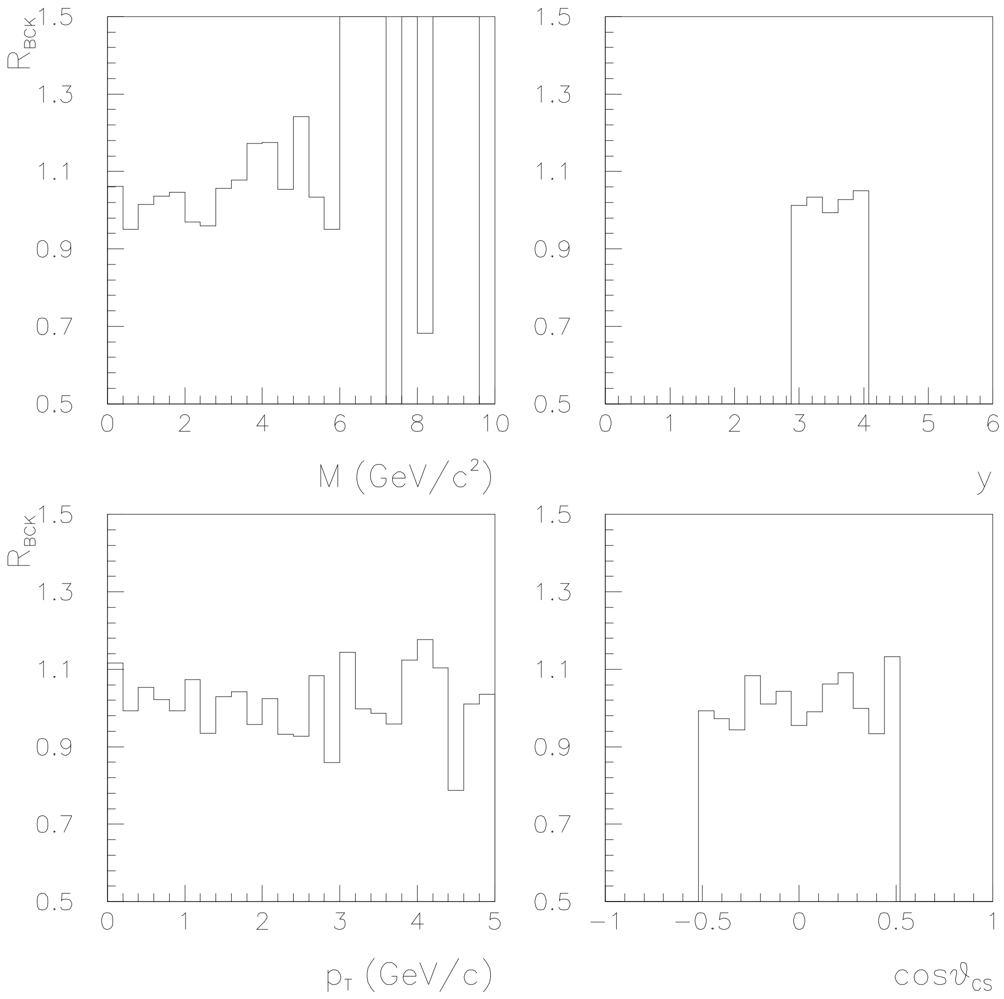

Figure 5.12: *Monte-Carlo R_{BCK} factor vs. dimuon mass, y, p_T and $cos\theta_{CS}$* after *kinematic cuts for peripheral (b=10 fm) Pb-Pb 158 A GeV/c events.*

System	b (fm)	$R \pm \sigma_R$
PbPb 158 A GeV/c	4	1.002 ± 0.005
PbPb 158 A GeV/c	7	1.004 ± 0.007
PbPb 158 A GeV/c	10	1.028 ± 0.013
PbPb 158 A GeV/c	13	1.073 ± 0.019
SU 200 A GeV/c	1	1.006 ± 0.003
SU 200 A GeV/c	4	1.007 ± 0.003
SU 200 A GeV/c	7	1.019 ± 0.003
SU 200 A GeV/c	10	1.069 ± 0.007

Table 5.2: *Monte-Carlo R_{BCK} factor obtained for the 4 impact parameter b values chosen for the PbPb and SU systems.*

$$\langle R_{Monte-Carlo} \rangle = \frac{\int dx \ \{\sum_{n=1}^{N_V} \sum_{i,j} P^{+-}(x)_{i,j}\}}{\int dx \ \{2\sqrt{(\sum_{n=1}^{N_V} \sum_{i,j} P^{++}(x)_{i,j})(\sum_{n=1}^{N_V} \sum_{i,j} P^{--}(x)_{i,j})}\}} \quad (5.22)$$

where $x = M, p_T, y, cos\theta_{CS}$. This average value is then used to correctly normalise the background contribution to the opposite-sign mass spectrum.

5.2.4 R_{BCK} centrality dependence

For the SU and PbPb systems the R_{BCK} factor has been computed for 4 different values of the impact parameter b, to investigate the R_{BCK} centrality dependence. In tab.5.2 the obtained R_{BCK} values are listed. As expected, R_{BCK} shows a marked dependence on centrality.

In fig.5.13 the points correspond to the 4 R_{BCK} values obtained in the Monte-Carlo simulation while the connecting curve is a fit to the Monte-Carlo points. For the PbPb system the value R_{BCK}=1.000 when $b = 0 \ fm$ has been imposed in order to avoid the use of too long CPU times.

We thus have a parametrisation of the R_{BCK} factor as a function of the impact parameter b for the two systems :

- PbPb 158 A GeV/c

$$R_{BCK} = 1.000 + 0.073 \cdot (b/13)^{4.04} \quad (5.23)$$

- SU 200 A GeV/c

$$R_{BCK} = 1.006 + 0.063 \cdot (b/10.)^{4.43} \quad (5.24)$$

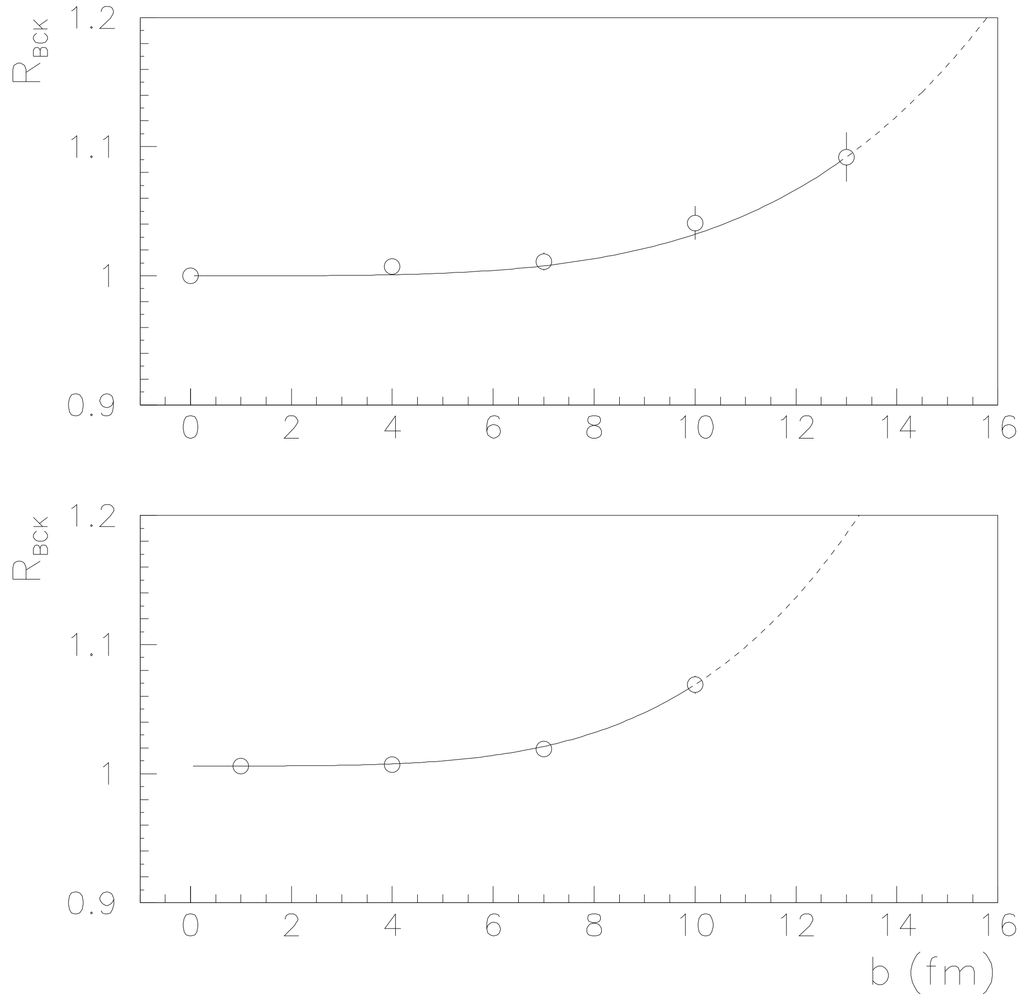

Figure 5.13: *Calculated R_{BCK} factor vs. impact parameter b for Pb-Pb collisions at 158 GeV per nucleon (top) and for S-U at 200 GeV per nucleon (bottom). The curves are fits to the Monte-Carlo points (plus an added point at b=0 fm for the PbPb system to which has been imposed a corresponding R_{BCK} value of* 1.000 ± 0.000*).*

In fig.5.14 the correlations between the impact parameter b and the transverse energy E_T are shown as obtained from the model described in[1], taking into account realistic nuclear densities.

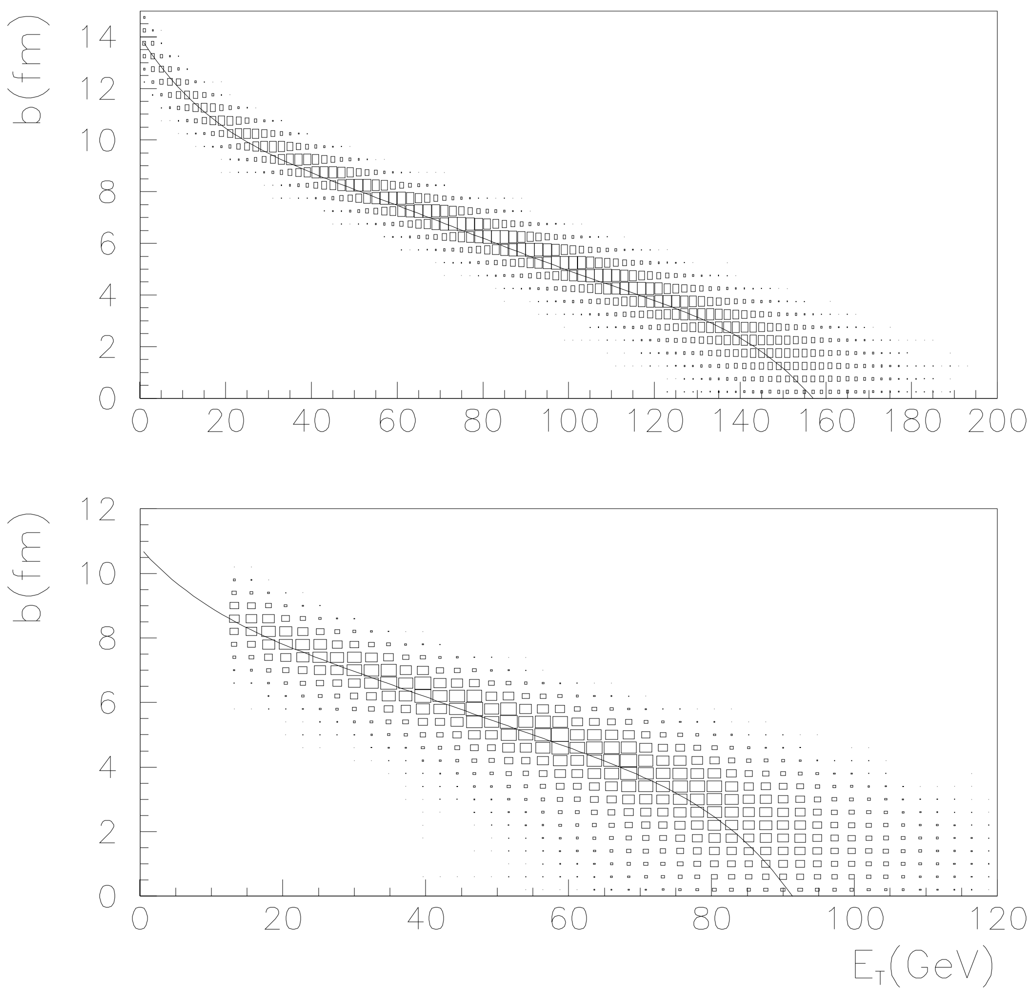

Figure 5.14: *Correlation between impact parameter b and transverse energy E_T for the PbPb 158 A GeV/c (top) and SU 200 A GeV/c (bottom) systems as obtained from[1].*

Each b vs. E_T correlation can be parametrised with a 5^{th} degree polynomial. The coefficients for the two polynomials corresponding to the PbPb and SU systems are listed in tab.5.3.
From the R vs. b and b vs. E_T correlations, the R vs. E_T one can be deduced, as it is shown in fig.5.15 where the centrality bins used in the PbPb and SU analysis are also indicated. To obtain the average $\langle R_{BCK} \rangle$ factor corresponding to a particular E_T bin, a weighted average over the events in that centrality bin is then performed, i.e., the distribution dN/dE_T vs. E_T is extracted from the data for each of the PbPb

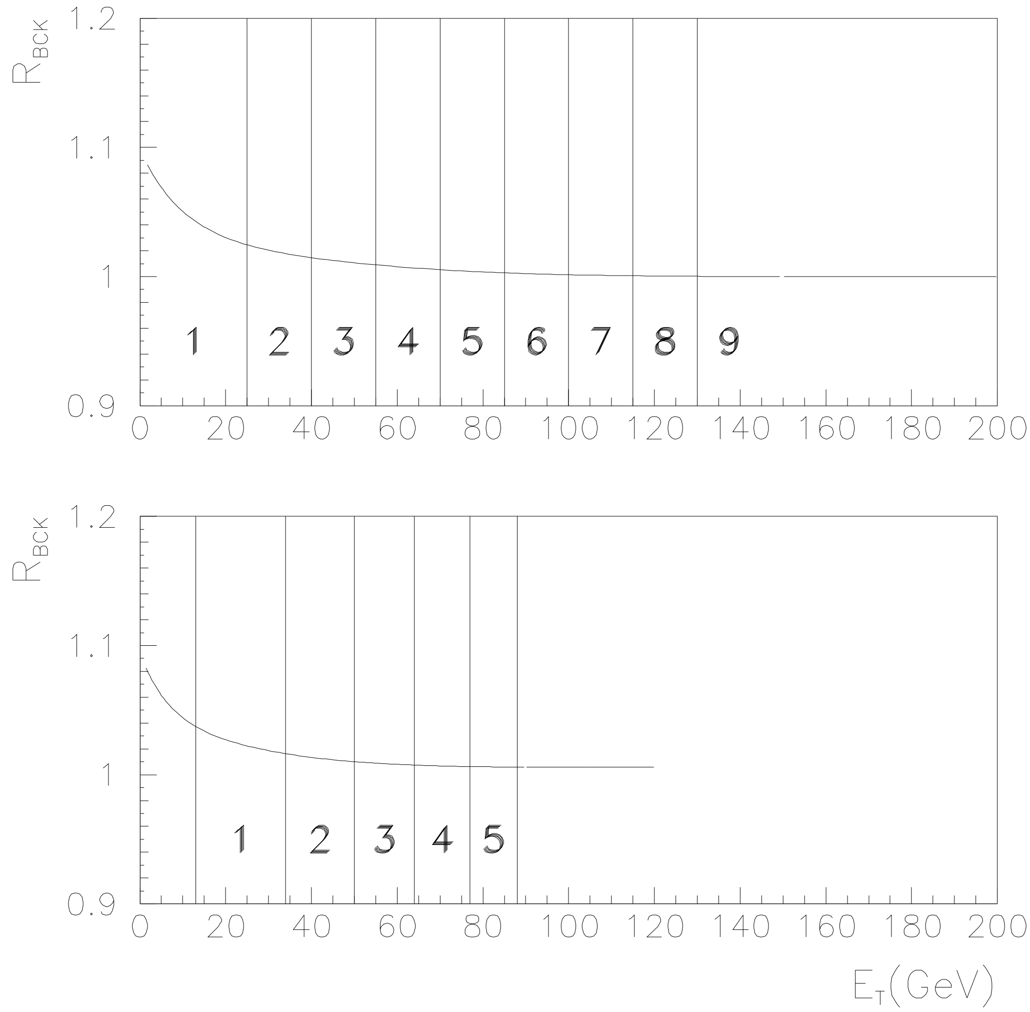

Figure 5.15: *Calculated R_{BCK} factor vs. transverse energy E_T for the PbPb 158 A GeV/c (top) and SU 200 A GeV/c (bottom) systems. See text for more details.*

		PbPb	SU
a_0 (10^0)	(fm)	$13.990 \pm 0.2\ 10^{-4}$	$10.800 \pm 0.1\ 10^{-4}$
a_1 (10^0)	(fm/GeV)	$-0.260 \pm 0.1\ 10^{-6}$	$-0.251 \pm 0.7\ 10^{-6}$
a_2 (10^{-2})	(fm/GeV^2)	$0.547 \pm 0.7\ 10^{-7}$	$0.798 \pm 0.4\ 10^{-5}$
a_3 (10^{-4})	(fm/GeV^3)	$-0.731 \pm 0.5\ 10^{-7}$	$-1.842 \pm 0.2\ 10^{-4}$
a_4 (10^{-6})	(fm/GeV^4)	$0.469 \pm 0.3\ 10^{-7}$	$2.113 \pm 0.8\ 10^{-4}$
a_5 (10^{-8})	(fm/GeV^5)	$-0.115 \pm 0.2\ 10^{-7}$	$-0.963 \pm 0.9\ 10^{-4}$

Table 5.3: *Coefficients of the 5^{th} degree polynomials parametrising the b vs. E_T correlations for the PbPb and SU systems.*

and SU E_T bins and the corresponding R_{BCK} value is computed for each of the E_T values in the bin; the R_{BCK} values are then weighted using the dN/dE_T distribution to obtain the final dN/dR_{BCK} one, where

$$\frac{dN}{dR_{BCK}^{Monte-Carlo}} dR_{BCK}^{Monte-Carlo} = \frac{dN}{dE_T} dE_T \tag{5.25}$$

If ΔR_{BCK} is the bin in the R_{BCK} variable corresponding to a particular E_T bin, the average value of R_{BCK} in that bin is

$$\langle R_{BCK}^{Monte-Carlo} \rangle = \frac{\int_{\Delta R_{BCK}} \{ R_{BCK}^{Monte-Carlo} \frac{dN}{dR_{BCK}} dR_{BCK} \}}{\int_{\Delta R_{BCK}} \{ \frac{dN}{dR_{BCK}} dR_{BCK} \}} \tag{5.26}$$

5.2.5 Pile-up effects

Combinatorial background dimuons are usually thought as being the combination of muons from $\pi's$ and $K's$ produced in a single interaction. This is correct only in the case where no pile-up effects exist. The pile-up of projectiles interacting in the same trigger time window leads to an overlapping of consecutive events. As a result, the detected dimuons can be combinations of muons generated in different events. During the SU and PbPb data taking periods, the Beam Hodoscope detected the incoming ions and signalled if more than one ion fell in the 20 ns trigger time window. Because of this $a-priori$ beam pile-up rejection, the pile-up effects can be thus neglected. It is instead mandatory to calculate their impact on the final R_{BCK} factor values in the case of the NA50 high intensity pA data taking periods, where no pile-up rejection was applied. To take the pile-up effect into account the following reasoning can be used [6] :

every time a good trigger is detected by the NA50 Hodoscopes, a 20 ns gate is opened. If we assume that the incoming projectile distribution follows the Poisson law, the probability of not having beam pile-up in the time window Δt is

$$P(0) = e^{-\overline{n}} \tag{5.27}$$

where $\overline{n}$ is the mean number of ions in the time interval Δt,

$$\overline{n} = \Delta t \cdot \frac{I}{B} \tag{5.28}$$

where I is the beam intensity (number of incident projectiles per burst) and B is the burst time length (effective-spill).
To compute the pile-up effects in the frame of our simulation, we proceed as follows : every-time an event is processed we randomly extract from the Poisson distribution

the number of projectiles which could pile-up. Taking into account the target thickness, the number N_{pu} of piling-up projectiles which actually interact in the target is computed.
Kaons and pions from the N_{pu} piling-up consecutive events are then combined. Again, every single kaon/pion is combined in all possible ways with all the kaons and pions in the sample of mesons from all the piling-up events. The previous procedure is then applied as in the case of no pile-up.

5.2.6 Results

In table 5.6, 5.4, 5.5 the R_{BCK} factors are shown for all the studied systems. In table 5.4 the pA low intensity R values are compared with the ones obtained taking into account the pile-up effects existing at the used experimental high intensity of $\simeq 2.5$ 10^9 p/burst. At higher intensities the R_{BCK} factor value becomes smaller because charge correlation effects are smeared out by the piling-up of different events.
The pW 200 GeV/c NA38 system has also been studied in the aim of cross checking with the R factor already obtained for that system in a previous analysis[3] developed within the NA38 Collaboration. The R_{BCK} factor value for the pW 200 GeV/c system had been measured on two sets of data collected with two slightly different hadron absorber set-ups.[3]. The signal distributions for the two pW set-ups had to be the same, whilst the measured background distributions were expected to reflect the difference between the used hadron absorber. A simultaneous fit of the two mass spectra was therefore performed, leaving the common R_{BCK} factor as a free parameter in the fit. The R_{BCK} factor obtained in that previous analysis is,

$$R_{BCK}\mid_{pW200}= 1.19 \pm 0.04 \tag{5.29}$$

to be compared with the one obtained in the present one,

$$\langle R\rangle \mid_{pW200}= 1.21 \pm 0.02 \tag{5.30}$$

The results obtained with the two different methods appear to be consistent; this gives as confidence in the reliability of our Monte-Carlo simulation.

In the following chapter, the pA, SU and PbPb sets of data are analysed and it is shown that when letting the R_{BCK}'s as free parameters in the fit or when imposing R_{BCK}=1 for all nucleus-nucleus systems, the risk of an unpredictable under or overestimation of the background exists. Therefore, the R_{BCK} factors listed in tab. 5.6, 5.4, 5.5 have been used to fix the background normalisation.

System	Energy (GeV/c)	$R \pm \sigma_R$ (low intensity)	$R \pm \sigma_R$ (I=2.5·10^9p/burst)	$R \pm \sigma_R$ (measured)
pW	200	1.21±0.02		1.19±0.04
pAl	450	1.19±0.05	1.06±0.02	
pCu	450	1.26±0.04	1.06±0.02	
pAg	450	1.21±0.04	1.06±0.01	
pW	450	1.21±0.03	1.05±0.01	

Table 5.4: *R factor for the pA systems. The high-intensity R_{BCK} values have been computed including the pile-up effect as explained in the previous paragraph. The pW 200GeV/c has been included to compare with the R_{BCK} factor obtained in the analysis of the two NA38 pW systems[3].*

System	Energy ($A\ GeV/c$)	E_T bin	E_T interval (GeV)	$R \pm \sigma_R$
PbPb	158	1	$E_T < 25$	1.035 ± 0.011
PbPb	158	2	$25 < E_T < 40$	1.017 ± 0.003
PbPb	158	3	$40 < E_T < 55$	1.010±0.002
PbPb	158	4	$55 < E_T < 70$	1.006±0.001
PbPb	158	5	$70 < E_T < 85$	1.003±0.0006
PbPb	158	6	$85 < E_T < 100$	1.001±0.0003
PbPb	158	7	$100 < E_T < 115$	1.001±0.0002
PbPb	158	8	$115 < E_T < 130$	1.000±0.0001
PbPb	158	9	$E_T > 130$	1.000±0.000

Table 5.5: *R_{BCK} factor for the 9 E_T bins of the PbPb 158 A GeV/c system. The error on R_{BCK} comes from the fit to the 4 (+1 imposed for b=0 fm) R_{BCK} Monte-Carlo values vs. b.*

System	Energy ($A\ GeV/c$)	E_T bin	E_T interval (GeV)	$R \pm \sigma_R$
SU	200	1	$13 < E_T < 34$	1.023 ± 0.005
SU	200	2	$34 < E_T < 50$	1.013 ± 0.002
SU	200	3	$50 < E_T < 64$	1.009 ± 0.0007
SU	200	4	$64 < E_T < 77$	1.007 ± 0.0004
SU	200	5	$77 < E_T < 88$	1.006 ± 0.0001

Table 5.6: *R factor for the 5 E_T bins of the SU 200 A GeV/c system. The error on R_{BCK} comes from the fit to the 4 R_{BCK} Monte-Carlo values vs. b.*

Bibliography

[1] Frederic Fleuret, PhD thesis, April 1997, Paris

[2] "Study of the estimation of the combinatorial muon pair background"- S. Constantinescu, S. Dita and D. Jouan, NA50 Collab.

[3] Carlos Lourenço, PhD thesis, January 1995, Lisbon

[4] K.Werner, Phys.Rep. 232(1993)87.

[5] GEANT-Detector Description and Simulation Tool-CERN Geneva(CH).

[6] "The correct way to calculate pileup"-C.Gerschel-NA50 Collab.